A LiDAR-Based Method to Identify Vegetation Encroachment in Power Networks with UAVs

Antonis Savva, Manos Papageorgiou, Christos Kyrkou, Panayiotis Kolios,
Theocharis Theocharides and Christos Panayiotou

Abstract—Vegetation encroachment in power transmission and distribution networks constitutes a major hazard for the environment and the networks' integrity, but also for the society at large, with multifaceted consequences. On many occasions the vegetation near the power lines, in conjunction with the aged infrastructure, caused and spread fires leading to large-scale disasters. To this end, 3D representations are proactively created using LiDAR sensors to identify locations of vegetation encroachment. Of particular interest is the use of UAVs, which propose a cost-effective alternative to employing airplanes. In this study, UAVs were employed to acquire LiDAR data from the power distribution network and a subtractive data-driven methodology is proposed, whereby irrelevant points are discarded, aiming to identify power lines without employing 3D modelling methods. In this context, geometric features are calculated and a rigorous analysis is conducted over the feature set, different classifiers and parameters to investigate the robustness of the proposed approach. Extensive evaluation suggests that the Random Forest classifier is able to identify power lines with high performance (*F1*-Score=97.74% and Accuracy=99.09%), using both geometric and color-based features, being also robust to the presence of moderate noise and down-sampling levels.

Index Terms—unmanned aerial vehicles, point cloud, 3D model, power line corridor, vegetation monitoring

I. INTRODUCTION

Modern societies rely on electricity to a profound extent; thus, urging Electricity Authorities (EAs) to expand and implement efficient mechanisms to monitor and maintain the existing infrastructure. The operated power transmission and distribution networks, which are most commonly aged, usually traverse large forest and mountainous regions, and are frequently exposed to adverse weather conditions [1], [2].

According to a recent report, many fires were caused and spread by the power infrastructure due to its adjacency to trees, with 100,000 hectares being burned during the California fires in 2018, while the blown fuses on a utility pole have sparked the Dixie fire in July 2021, resulting in 400,000 burned hectares. The effects were immense both financially and socially but also environmentally, with hundreds of structures being destroyed and a town being vanished almost in its entirety. Simultaneously, the released smoke endangered the health of millions of people [3].

Consequently, it is critical to apply preemptive measures to prevent such disasters. To this end, EAs employ skilled personnel which either on foot or with helicopters are dispatched across the infrastructure to monitor the vegetation and identify high-risk locations [4]. Although this approach has been used for decades, it is accompanied by increased workload and long inspection cycles, while the accuracy is greatly dependent on the inspectors' observation skills [2], [4].

In this context, Light Detection and Ranging (LiDAR) airborne scanning technology is the ideal alternative for creating accurate 3D models of the power lines and is preferred to Mobile- and Terrestrial- Laser Scanning methods, which cannot be applied in dense forest and steep mountainous landscapes [2], [5]. Additionally, during the last few years, Unmanned Aerial Vehicles (UAVs) have been made widely available, proposing a low cost and flexible solution for power infrastructure inspection applications covering the entire spectrum of power components [6], [7], power line [8], [9], utility poles detection [10], [11], as well as the development of autonomous systems to rapidly acquire high-quality data in a repeatable manner using multiple sensors, e.g. RGB, thermal, multispectral [12], [13].

In this study, a LiDAR-enabled UAV is employed to acquire 3D data from the power distribution network and an algorithm is developed to identify vegetation encroachment in the power lines. The main contributions include:

- A subtractive methodology is proposed to identify the power lines, by gradually discarding irrelevant points based on 3D geometrical characteristics. In doing so, we aim to avoid developing methods to directly detect the power lines in the initial point cloud, with potentially increased time complexity.
- A data-driven approach is proposed to detect the power lines avoiding the use of 3D line fitting and modelling methods.
- A rigorous analysis is performed to test the resilience and robustness of the proposed algorithm for different classification algorithms, feature combinations, as well as noise and down-sampling levels.

The rest of the paper is structured as follows: Section II illustrates the related work, while the description of the proposed methodology is given in Section III. The rigorous

analysis of proposed method is presented in Section IV, while concluding remarks are presented in Section V.

II. RELATED WORK

In one of the first studies, a methodology was proposed to classify points into power lines, vegetation and surfaces [14]. This was achieved by defining ellipsoid neighborhoods and calculating the covariance matrix, whose eigenvalues indicate data spread. Finally, for classification a Gaussian mixture model was trained using the expectation-maximization algorithm [14]. In another study, a multi-stage method was proposed using Markov Random Field classifier to distinguish power lines using linear features, while non-linear features were employed to classify buildings and other objects [15]. Subsequently, electric towers were localized to facilitate the detection of conductor spans, i.e. power lines between two towers, and apply 3D catenary curve models. The inclusion of points representing the power lines was established through a hypothesis-verification approach [15]. In contrast, in [16] a methodology was developed to analyze vegetation based on geometric features, by detecting trees near the infrastructure, while a Random Forest classifier was used to classify tree species. As a result, trees growing within the safe distance and tall trees that could fall onto the power lines were identified.

Efforts in [17] concentrated on improving the classification performance by calculating 26 features encoding the local point cloud geometry in conjunction with the JointBoost supervised algorithm. This approach was applied on two point clouds for distinguishing ground, vegetation, buildings, power lines and pylons, obtaining accuracy of 95.73% and 93.88%, while graph-cut segmentation was employed to increase accuracy to 97.48% and 95.03%, respectively [17]. On the other hand, in [18] ground and trees were identified based on calculation of geometric features using a variety of different neighborhood types and scales, suggesting that improved classification performance can be obtained with multi-type and multi-scale approaches, compared to single-type and single-scale alternatives. Along similar lines, in [19] Support Vector Machines were employed and a variety of geometric features were calculated considering multi-scale neighborhood schemes; thus, achieving precision rates of 95.64% and 93.83%, with the recall rates being 90.92% and 89.09% in two point clouds, respectively.

In [20], geometric characteristics were calculated to detect pylons, vegetation and power lines, while the Euclidean distance algorithm was used to cluster the power lines at different heights. The final separation was performed through a 2D line fitting procedure following a planar projection. Similarly, the Hough transform was used to distinguish power lines from noise and surrounding vegetation [5]. Additionally, in [21] a 7-fold pipeline was proposed consisting of: initial pylon and power lines classification, separation of individual pylons, classification of shields and power lines, identification of insulators, classification of shield wire endings and chains, and finally catenary modelling. In this context, power lines were identified and categorized into three subclasses, i.e. shield conductors, common conductors and chains, while pylon classification was performed into suspension and anchor pylons.

Convolutional Neural Networks have been also employed to classify full-waveform airborne LiDAR data [22]. A two-step methodology was followed aiming to initially pre-process data from each waveform to a compact representation, which along with coordinates of the points were mapped to an image. The resulting image was fed into a Fully Convolutional Network for segmenting it into six classes, i.e. ground, vegetation, building, power line, tower and street path, achieving an accuracy of 92.6% [22].

Towards real-time classification, a method was presented in [23], harnessing the capabilities of edge computing and data transmission through the 4G network. With the processing being made during the UAV flight, risk assessment reports were generated in a timely manner to facilitate prompt response of inspection personnel. Likewise, in [24] a large point cloud was divided into smaller segments to improve processing time, while a voxel grid filter was applied for separating power lines, pylons and vegetation. Subsequently, points representing power lines were converted to binary images for retrieving individual spans, which in turn were used to identify nearby vegetation.

In [25], a fully automatic approach was presented for extracting the power lines and measuring the distance to the closest tree. The proposed methodology included geometrical analysis and, in terms of a knowledge-based approach, the points on the power lines were isolated from those representing other structures, i.e. vegetation and towers. Finally, a 3D line following approach was employed to select all the points on the power lines using an automatically selected seed point, whose selection greatly affected algorithm's performance. Apart from the aforementioned approaches, methodologies have been proposed based on detecting trees using site-specific thresholds and employing growth models to predict and facilitate early detection of tree encroachment [2].

In this context, the present study proposes a subtractive data-driven methodology, using a combination of conventional geometrical reasoning through calculation of 3D geometric features and machine learning approaches to detect power lines, without employing additional power line fitting methods, e.g. 3D catenary curve models. Specifically, instead of directly identifying power lines in the initial point cloud, the proposed approach consists of extracting irrelevant points to reduce computational complexity, by leveraging on geometrical information of the 3D scene. Consequently, only the power lines remain along with surrounding vegetation; thus, reducing to a binary classification problem, i.e. "power lines" vs "other points". Additionally, a rigorous analysis is performed through an exhaustive search of geometric features across a variety of classifiers, under different noise and down-sampling levels, to investigate the robustness of the proposed approach.
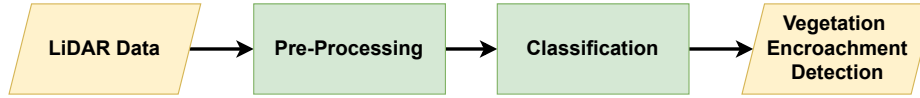
Fig. 1: Process diagram for identifying power lines and high-risk locations of vegetation encroachment

III. METHODOLOGY

A. Equipment and Data Acquisition

The DJI Matrice 300 Real Time Kinematics (RTK) UAV was employed (https://www.dji.com/matrice-300), along with the DJI Zenmuse L1 camera (https://www.dji.com/zenmuse-l1), as shown in Fig. 2. As a testing site, a part of the medium voltage network in Cyprus was considered with length of 800m, consisting of 9 utility poles, with the UAV performing an autonomous flight at a height of 50m above ground, navigating directly above each pole. This was achieved by applying an autonomous mapping procedure prior to LiDAR data acquisition, using the ICARUS system [13]. It must be noted that the use of a quadcopter is not specific to the proposed methodology and fixed-wing UAVs, capable of carrying LiDAR sensor, can be used as well.

Specifically, the UAV was provided with the best estimates of the utility poles' coordinates and navigated to these positions. As soon as each location was reached, a real-time detection process was initiated to detect top-view of the pole using video feed from the RGB camera and the tiny-You-Only-Look-Once (tiny-YOLO) v4 [26]. Detection output, i.e. bounding box marking the pole, was subsequently integrated with the UAV's flight controller, facilitating the generation of suitable control commands for aligning the UAV directly above the pole. To promote high navigation and positioning accuracy multi-frequency and multi-constellation Global Navigation Satellite Systems (GNSSs), e.g. GPS, Galileo, GLONASS, and BeiDou, were enabled on the employed UAV [13].

B. LiDAR Sensor Setup

LiDAR was configured to acquire data using triple-echo mode, i.e. for each laser pulse up to three reflections were received, at a frequency of 160kHz, while the repetitive scanning pattern was selected with $FOV = 70.4° \times 4.5°$; thus, acquisition was performed in horizontal stripes for improved representation accuracy. Moreover, RGB images were acquired throughout the UAV's flight and were processed in conjunction with raw LiDAR data with the DJI Terra software (https:

Fig. 2: UAV and LiDAR sensor used for acquiring data

//www.dji.com/dji-terra) to obtain a colored 3D representation of the power infrastructure. This colored point cloud was set as input to the proposed methodology for identifying the power lines and detecting high-risk locations of vegetation encroachment, as depicted in Fig. 1.

C. Pre-processing

Pre-processing aims at discarding irrelevant points, since we are interested in the power lines and the vegetation close to them, to minimize computational complexity and promote higher detection performance, compared to directly comparing power lines in the initial point cloud. The following pre-processing steps were performed in the PDAL library (https://pdal.io/en/2.5.2/) as described in the diagram in Fig. 3-left panel and shown in Figs. 4b-4g.

1) ScanAngle-Based Filtering: Considering that the UAV navigated directly above the utility poles, the power lines were in the middle of the dataset; thus, points on the left and right can be discarded. As mentioned above, the horizontal FOV of the LiDAR sensor is 70.4°, i.e. $ScanAngle \in$ [-35.2°, 35.2°] (Fig. 4b), and the power lines were found for $ScanAngle \in [-10°, 10°]$ (Figs. 4c-4d).

2) Down-Sampling: Uniform down-sampling was applied to reduce the number of points using a voxel-based method with cell size of $[V_x, V_y, V_z] = [.2, .2, .2]m$, whereby points within each cell were replaced by the point being nearest to the cell's center (Fig. 4e).

3) Ground Filtering: To classify terrain the Simple Morphological Filter algorithm was employed, through which a minimum surface was created and processed to distinguish grid cells containing bare earth and objects. Subsequently, a digital elevation model was produced to facilitate identification of ground points on the original LiDAR data [27] (Fig. 4f).

4) Outliers Detection: Sparse outliers were removed through a statistical outlier removal method, by computing for each query point $\boldsymbol{p}_q = [x_q, y_q, z_q]^T$ in the point cloud $\mathcal{P}$, the distances to its k-nearest neighbors and subsequently calculating their mean μ_q and standard deviation σ_q. A point was then considered as an outlier if its corresponding μ_q value fell outside $\mu_q \pm \alpha \cdot \sigma_q$, where $\alpha = 2.0$ and $k = 8$ [28] (Fig. 4g).

D. Classification

Classification aims to distinguish power lines from the remaining points (mainly vegetation) and consists of three main steps as described in Fig. 3-right panel and presented in Figs. 4h-4j.
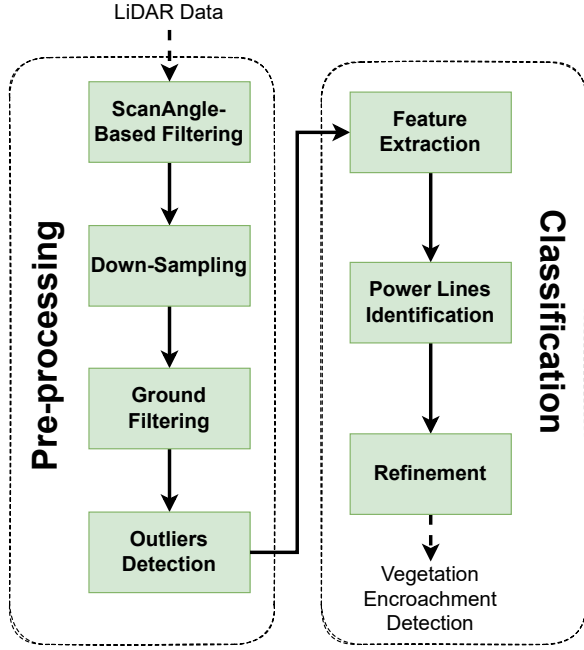
LiDAR Data

Fig. 3: Pre-processing steps for removing points not corresponding to power lines and classification procedure

1) Features Extraction: A total of 16 features were computed (Table I and Fig. 4h). Apart from *R*, *G*, *B* and *Intensity* features which correspond to RGB values and reflectivity of the laser beam, respectively, the rest aim to provide local geometric characteristics of $\mathcal{P}$, based on the covariance matrix $\mathcal{C}_q \in \mathbb{R}^{3\times3}$, which was calculated for each query point $\boldsymbol{p}_q$ using its k-nearest neighbors as follows [29]:

$$\mathcal{C}_q = \frac{1}{k-1}\sum_{i=1}^{k}(\boldsymbol{p}_i - \overline{\boldsymbol{p}})\cdot(\boldsymbol{p}_i - \overline{\boldsymbol{p}})^T \ , \ \overline{\boldsymbol{p}} = \frac{1}{k}\sum_{i=1}^{k}\boldsymbol{p}_i \quad (1)$$

with $\overline{\boldsymbol{p}}$ representing the geometric center.

Covariance matrix $\mathcal{C}_q$ is symmetric and positive semi-definite with its eigenvectors $\vec{v}_j$ forming an orthogonal frame and its eigenvalues being positive real numbers $\lambda_j \geq 0 \in \mathbb{R}$, $j \in \{0,1,2\}$ [30]. By sorting the eigenvalues as $\lambda_2 \geq \lambda_1 \geq \lambda_0 \geq 0$ the geometric features were calculated as shown in Table I [29], [31]–[33]. Additionally, the eigenvector $\vec{v_0}$ which corresponds to the smallest eigenvalue λ_0, is an approximation of the local surface normal $\vec{n} = [n_x, n_y, n_z]$ [34].

2) Power Lines Identification: For distinguishing the power lines, a binary classification problem was defined, i.e. "power lines" vs. "other points" (Fig. 4i). In this context, 9 classification algorithms were examined, i.e. AdaBoost, Decision Tree (DecTree), Extra Tree (ExtTree), Gaussian Mixture (Gauss-Mix), KMeans, KMeans Mini Batch (KMeansMB), Linear Support Vector Classifier (LinearSVC), Logistic Regression (LogRegr) and Random Forest (RandFor). All classifiers were implemented using scikit-learn library (https://scikit-learn.org/1.2/) and in-house code. To assess the performance of classification a stratified 5-fold cross validation scheme was estab-

TABLE I: Calculated geometric features for classifying power lines

Features	Definition
R	Value corresponding to Red channel
G	Value corresponding to Green channel
B	Value corresponding to Blue channel
Intensity	Reflectivity of the laser beam
Height above Ground	Initially a Delaunay triangulation is created using M ground points closest to the non-ground query point $\boldsymbol{p}_q$. If $\boldsymbol{p}_q$ lies inside the triangulated area, the assigned value is $Z_q - Z_{tr}$, where Z_{tr} is the result of interpolation from the three triangle vertices. Otherwise, the assigned value is $Z_q - Z_{cl}$, where Z_{cl} is the value of the nearest ground point [31].
Linearity	$L_\lambda = (\lambda_2 - \lambda_1)/\lambda_2$
Planarity	$P_\lambda = (\lambda_1 - \lambda_0)/\lambda_2$
Scattering	$S_\lambda = \lambda_0/\lambda_2$
Anisotropy	$A_\lambda = (\lambda_2 - \lambda_0)/\lambda_2$
Omnivariance	$O_\lambda = \sqrt[3]{\lambda_0\lambda_1\lambda_2}$
Eigentropy	$E_\lambda = -\sum_{i=0}^{2}\lambda_i\ln(\lambda_i)$
Sum of eigenvalues	$\Sigma_\lambda = \sum_{i=0}^{2}\lambda_i$
Surface Variation	$C_\lambda = \lambda_0/(\lambda_0 + \lambda_1 + \lambda_2)$
Demantke's Verticality	$V_D = 1 - n_z$
Guinard's Verticality	$V_G = \hat{n}_z$, i.e. the vertical component of $\hat{\boldsymbol{n}} = \sum_{i=0}^{2}\lambda_i\vec{\boldsymbol{v}_i}$
Density	$D = (k+1)/(\frac{4}{3}\pi r_{k-\mathrm{NN}}^3)$, with $r_{k-\mathrm{NN}}$ being the radius encapsulating the k-nearest neighbors.

lished, to construct the confusion matrix, shown in Table II, and calculate performance metrics as follows:

$$\begin{aligned} Accuracy &= \frac{TP + TN}{TP + TN + FP + FN} \\ Precision &= \frac{TP}{TP + FP} \\ Recall &= \frac{TP}{TP + FN} \quad (2)\\ F1\text{-}Score &= 2 \cdot \frac{Precision \cdot Recall}{Precision + Recall} \\ Jaccard &= \frac{TP}{TP + FP + FN} \end{aligned}$$

with TP, FP, TN and FN corresponding to True Positives, False Positives, True Negatives and False Negatives, respectively. Ground truth was established by manually assigning labels, i.e. power lines and other, to all points of the dataset, using CloudCompare (https://cloudcompare.org/).

TABLE II: Confusion Matrix

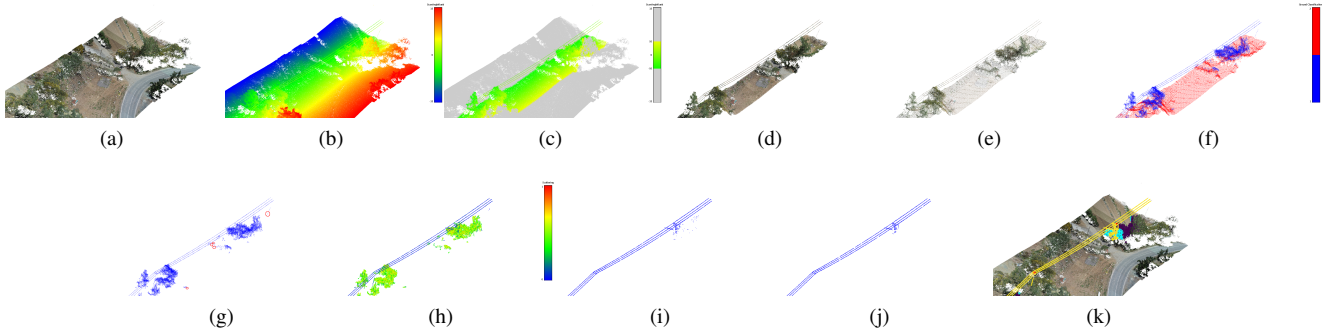|		PREDICTION	
		Power Lines	*Other*
GROUND	*Power Lines*	TP	FP
TRUTH	*Other*	FN	TN

Fig. 4: Procedure to identify locations of vegetation encroachment using LiDAR data: (a) initial LiDAR data, (b) horizontal scan angle, (c) power lines points are characterized by small scan angle values, (d) scan angle based filtering, (e) down-sampling, (f) ground filtering, (g) outliers detection, (h) feature extraction, (i) power lines identification, (j) refinement of identified power lines and (k) vegetation encroachment detection

3) Refinement: The identified power lines may also contain spurious detections; hence, to remove these outliers the method described in Section III-C4 was applied to refine the classification results (Fig. 4j).

IV. RESULTS

A. Classifier Assessment

As mentioned in Section III-D2, to assess classification performance a stratified 5-fold cross validation scheme was established, since only one dataset was available, and was selected over the simple 5-fold cross validation approach, as the former preserves the percentage of samples for each class; an important aspect since the points representing power lines were much fewer than the rest. Performance evaluation was based on a grid-search approach over the set of features, by calculating the binomial coefficients to define the subset of features to be used as input to the classifiers. Specifically, the number of combinations was calculated as follows:

$$\binom{16}{m} \, , \, m \in \{5, 6, 7, 8, 9, 10\} \tag{3}$$

resulting in 4368, 8008, 11440, 12870, 11440, and 8008, respectively, totalling 56134 feature combinations.

The corresponding results are shown in Fig. 5 in the form of 2D matrix. Rows correspond to the feature combinations starting from top to bottom, i.e. the upper part relates to all combinations of 5 features, the second are the combinations of 6 features etc. Colors correspond to the obtained *F1*-score through the stratified 5-fold cross validation scheme.

Some remarks can be made by observing Fig. 5: DecTree and ExtTree performed similarly, while GaussMix exhibited the lowest performance for a number of feature combination. KMeans yielded lower *F1*-scores when fewer features were used, albeit this was improved as additional features were considered. On similar grounds, KMeansMB exhibited low performance with fewer features, which increased with an increasing number of features. LinearSVC and LogRegr

performed similarly and consistently across the various feature combinations, while AdaBoost also achieved high performance. RandFor exhibited the highest classification score across all feature combinations, although it can be seen that in some cases performance was slightly decreased; nonetheless, it is the best performing classifier among the chosen ones. In Table III, the feature combination achieving the highest performance for each classifier is presented.

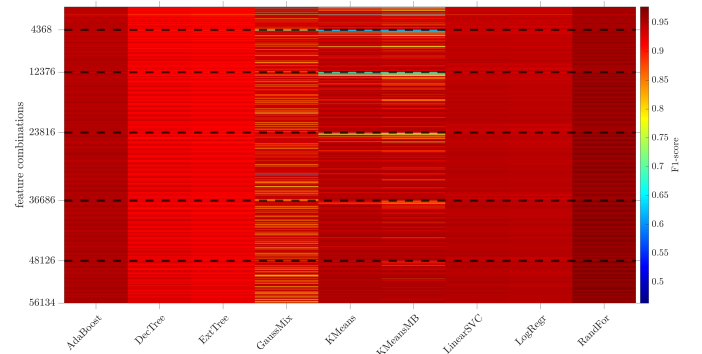Focusing on RandFor, the inclusion of additional features

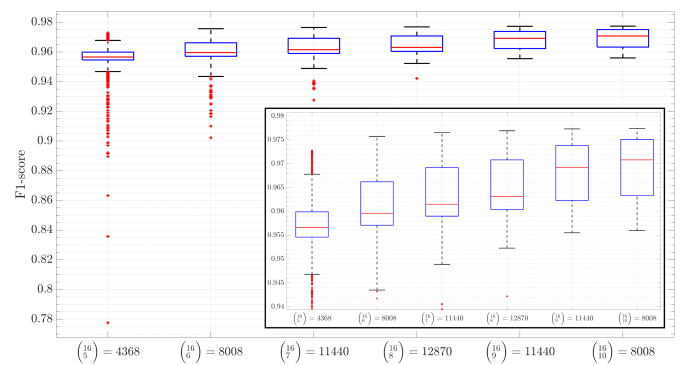Fig. 5: Performance of classifiers over all feature combinations

Fig. 6: Performance of RandFor classifier

TABLE III: Combination of features yielding the highest performance of each classifier

Classifier	Feature Combination	F1-Score	Accuracy	Precision	Recall	Jaccard
AdaBoost	Red, Blue, HeightAboveGround, Anisotropy, Density, Planarity, GuinardVerticality	0.9605	0.9845	0.9825	0.9419	0.9250
DecTree	Red, Blue, Intensity, HeightAboveGround, DemantkeVerticality, Eigenentropy, Omnivariance, SurfaceVariation	0.9402	0.9754	0.9361	0.9486	0.8874
ExtTree	Red, Blue, Intensity, HeightAboveGround, Omnivariance, Scattering, EigenvalueSum, GuinardVerticality	0.9375	0.9745	0.9372	0.9427	0.8828
GaussMix	Green, Blue, HeightAboveGround, Anisotropy, Eigenentropy, Omnivariance, SurfaceVariation	0.9510	0.9807	0.9904	0.9145	0.9065
KMeans	Blue, Intensity, HeightAboveGround, Eigenentropy, EigenvalueSum, SurfaceVariation	0.9644	0.9858	0.9917	0.9387	0.9313
KMeansMB	Blue, Intensity, HeightAboveGround, Anisotropy, Eigenentropy, EigenvalueSum	0.9640	0.9857	0.9885	0.9408	0.9306
LinearSVC	Green, Blue, HeightAboveGround, DemantkeVerticality, Eigenentropy, Omnivariance, Planarity, EigenvalueSum, SurfaceVariation, GuinardVerticality	0.9573	0.9833	0.9843	0.9346	0.9196
LogRegr	Red, Blue, HeightAboveGround, DemantkeVerticality, Eigenentropy, Linearity, Omnivariance, EigenvalueSum, SurfaceVariation, GuinardVerticality	0.9541	0.9817	0.9728	0.9396	0.9134
RandFor	**Red, Green, Blue, Intensity, HeightAboveGround, DemantkeVerticality, Planarity, Scattering, EigenvalueSum, GuinardVerticality**	**0.9774**	**0.9909**	**0.9949**	**0.9605**	**0.9558**

improves performance, as shown in Fig. 6. By selecting few features (5 and 6) the exhibited performance is not consistent, as suggested by the presence of outliers. On the other hand, the inclusion of 9 and 10 features improves the performance, whereby no outliers are observed suggesting that the included features better describe the 3D geometry; thus, allowing for more accurate and consistent classification outcomes. In Table IV, the feature combination achieving the highest performance for each number of features is presented. As can be seen, the combination of 10 features is marginally better compared to the remaining, as the addition of 1 feature at a time slightly improves the performance, in agreement with Fig. 6. Importantly, increasing the dimension of the feature set has negligible impact on training and testing time, as shown in Table IV, as well as in computational resources.

The performance of the remaining classifiers for the optimal feature combination, i.e. {*Red, Green, Blue, Intensity, HeightAboveGround, DemantkeVerticality, Planarity, Scattering, EigenvalueSum, GuinardVerticality*}, is illustrated in Fig. 7. The remaining classifiers exhibited lower performance. Notably, GaussMix yielded the highest precision, by *not* identifying FPs ("power lines" as "other points"). Also, recall was significantly lower, suggesting that a large number of FNs was identified ("other points" as "power lines"; Eq. 2).

B. Effect of Noise

Additive spatial Gaussian noise was generated as follows: $p_j^* = p_q + t_q$, with $t_q = [t_x^q, t_y^q, t_z^q] \sim \mathcal{N}(0, \sigma)$ and $p_q \in \mathcal{P}$, while the noisy point cloud was created by concatenation: $\mathcal{P}_{noisy} = \mathcal{P} \cup \mathcal{P}^*$. Noise was generated for evenly-spaced points, i.e. every 1m, 0.5m and 0.2m, corresponding to 0.35%, 1.38% and 7.9% of points, respectively. Moreover, standard deviation was altered using values: $\sigma \in \{0.1, 0.2, 0.3, 0.4, 0.5\}$. As can be seen in Fig. 8 (the horizontal dashed lines correspond to the performance

without artificially added noise) the presence of noise affected the performance to a different extent relating both with σ and spatiality. Specifically, a steep decline in performance is observed when points spaced 0.2m apart were affected by noise, compared to those spaced 1m, for all examined standard
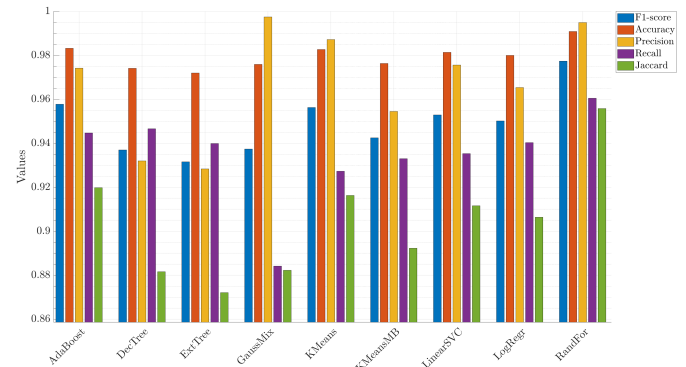

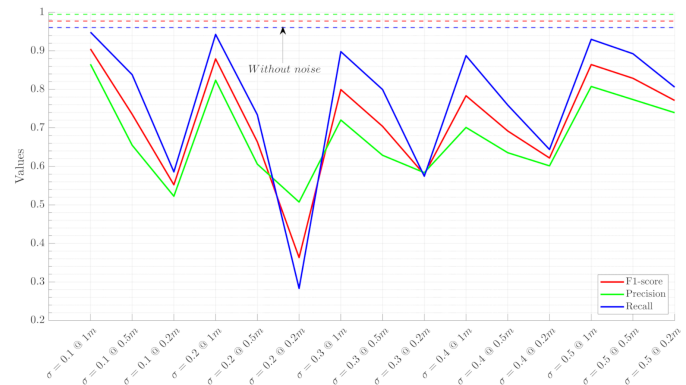Fig. 7: Comparison of classifiers for the optimal feature combination

Fig. 8: RandFor performance in the presence of noise

TABLE IV: Performance of Random Forest for each number of features combination

Feature Combination	F1-Score	Accuracy	Precision	Recall	Jaccard	Training Time (s)	Test Time (s)	Memory Used (MB)
Red, Blue, Intensity, HeightAboveGround, Anisotropy	0.9728	0.9891	0.9901	0.9561	0.9470	0.5215	0.2346	1046.125
Red, Blue, Intensity, HeightAboveGround, Scattering, GuinardVerticality	0.9757	0.9902	0.9922	0.9597	0.9526	0.5413	0.2360	1050.125
Green, Blue, Intensity, HeightAboveGround, DemantkeVerticality, Scattering, GuinardVerticality	0.9765	0.9905	0.9932	0.9603	0.9540	0.5285	0.2361	1050.125
Red, Blue, Intensity, HeightAboveGround, DemantkeVerticality, Omnivariance, SurfaceVariation, GuinardVerticality	0.9769	0.9907	0.9941	0.9602	0.9548	0.5466	0.2431	1050.125
Red, Green, Blue, Intensity, HeightAboveGround, DemantkeVerticality, Eigenentropy, Scattering, GuinardVerticality	0.9773	0.9909	0.9939	0.9612	0.9556	0.5891	0.2382	1050.125
Red, Green, Blue, Intensity, HeightAboveGround, DemantkeVerticality, Planarity, Scattering, EigenvalueSum, GuinardVerticality	**0.9774**	**0.9909**	**0.9949**	**0.9605**	**0.9558**	**0.5921**	**0.2423**	**1052.125**

deviation values. Through a closer look, it can be inferred that while precision is more stable compared to recall (meaning that "power lines" were classified as such), recall exhibits significantly lower performance, since "other points" were classified as "power lines". By construction, additive noise was also added near the power lines to the extent defined by values of σ; hence, these noisy points were considered for calculating covariance matrix due to their inclusion in the local neighborhoods. Nevertheless, results suggest that RandFor is robust in the presence of moderate noise (*F1*-score $> 90\% : \sigma = 0.1$ with $1m$ spacing), while extreme levels of noise are unlikely to be introduced in the data, since UAV LiDAR technology has significant improvements during the last years.

C. Effect of Down-Sampling

To examine the effect of different sampling rates, i.e. point density that may be obtained by using different LiDAR sensors, a variety of down-sampling rates have been tested in the voxel-based method (Section III-C2). Specifically, cells with sizes 0.1m, 0.3m, 0.4m and 0.5m were additionally considered. The alteration of down-sampling levels does not affect, in a negative manner, classification performance (Fig. 9). Interestingly, a slightly higher *F1*-score was obtained with larger
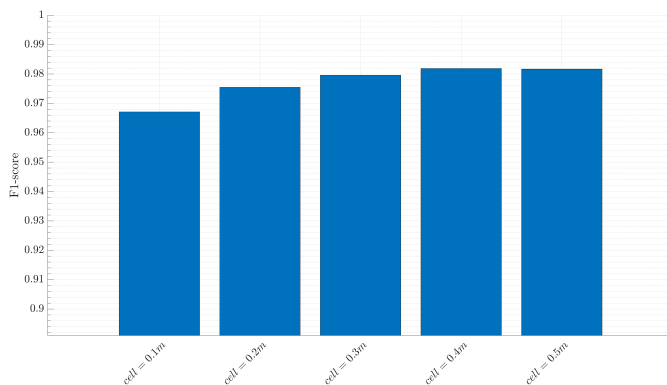

Fig. 9: RandFor performance for different down-sampling rates

cell sizes, which can be attributed to the specific geometry of the utility poles: the three power lines are horizontal and the space between them varies from 0.6m to 0.9m, depending on the location. Consequently, cell sizes up to 0.5m seem to *not* affect nearby power lines, i.e. two power lines in the same cell. Moreover, neighbors were spread in space; hence, geometric features were able to better capture the geometry of the 3D scene. These results suggest the potential of RandFor classifier, creating avenues to explore in a more detailed manner the link between down-sampling levels and parameters for estimating features, i.e. neighborhood size and type, with classification performance.

V. CONCLUSIONS AND FUTURE WORK

In this study, a LiDAR-enabled UAV was employed to acquire data from the medium voltage distribution network in Cyprus for identifying locations of vegetation encroachment. In particular, a subtractive data-driven methodology is proposed, whereby irrelevant points are initially discarded and then power lines are identified through a binary classification method ("power lines" vs "other"). In this context, a meticulous approach was applied over a wide selection of classifiers, geometric features, noise and down-sampling levels for analyzing the landscape of combinations and parameter selection, ultimately leading to the best performing combination. The obtained results suggest that Random Forest is the highest performing classifier (*F1*-score=97.74% and accuracy=99.09%), also exhibiting robustness in the presence of moderate noise and down-sampling levels. With regards to the optimal feature set, this consisted of both of color and intensity information, as well as geometric characteristics of the point cloud.

As a future work we are planning to acquire more point cloud data under different scenarios, i.e. forest and plain areas with no vegetation near the power lines and cases where it is much closer, i.e. touching the power lines. Consequently, the proposed method will be assessed and verified in these diverse conditions; thus, defining the corresponding robustness levels of the application. Ultimately, locations of vegetation

encroachment will be identified on time, allowing operators to proceed to proper measures to maintain safety of the power network.

VI. Acknowledgment

References

[1] L. Matikainen, M. Lehtomäki, E. Ahokas, J. Hyyppä, M. Karjalainen, A. Jaakkola, A. Kukko, and T. Heinonen, "Remote sensing methods for power line corridor surveys," *ISPRS Journal of Photogrammetry and Remote Sensing*, vol. 119, pp. 10–31, 2016.

[2] Y. Chen, J. Lin, and X. Liao, "Early detection of tree encroachment in high voltage powerline corridor using growth model and UAV-borne LiDAR," *International Journal of Applied Earth Observation and Geoinformation*, vol. 108, p. 102740, 2022.

[3] V. Chaudhry, "Smokey the AI." IEEE Spectrum, Available at https://spectrum.ieee.org/smokey-the-ai, 19 Oct 2021.

[4] V. N. Nguyen, R. Jenssen, and D. Roverso, "Automatic autonomous vision-based power line inspection: A review of current status and the potential role of deep learning," *International Journal of Electrical Power & Energy Systems*, vol. 99, pp. 107–120, 2018.

[5] N. Munir, M. Awrangjeb, and B. Stantic, "Extraction of forest power lines from LiDAR point cloud data," in *2021 Digital Image Computing: Techniques and Applications (DICTA)*, pp. 01–06, 2021.

[6] R. Ye, Q. Wang, B. Yan, and B. Li, "Position and orientation detection of insulators in arbitrary direction based on YOLOv3," in *Pattern Recognition and Computer Vision* (Y. Peng, Q. Liu, H. Lu, Z. Sun, C. Liu, X. Chen, H. Zha, and J. Yang, eds.), (Cham), pp. 551–563, Springer International Publishing, 2020.

[7] T. Li, J. Zhou, G. Song, Y. Wen, Y. Ye, and S. Chen, "Insulator infrared image segmentation algorithm based on dynamic mask and box annotation," in *2021 11th International Conference on Power and Energy Systems (ICPES)*, pp. 432–435, 2021.

[8] V. N. Nguyen, R. Jenssen, and D. Roverso, "LS-Net: fast single-shot line-segment detector," *Machine Vision and Applications*, vol. 32, p. 12, Oct 2020.

[9] H. Choi, J. P. Yun, B. J. Kim, H. Jang, and S. W. Kim, "Attention-Based multimodal image feature fusion module for transmission line detection," *IEEE Transactions on Industrial Informatics*, vol. 18, no. 11, pp. 7686–7695, 2022.

[10] A. Cerón, I. Mondragón, and F. Prieto, "Real-time transmission tower detection from video based on a feature descriptor," *IET Computer Vision*, vol. 11, no. 1, pp. 33–42, 2017.

[11] S. Zhang, B. Chen, R. Wang, J. Wang, L. Zhong, and B. Gao, "Unmanned aerial vehicle (UAV) vision-based detection of power line poles by CPU-based deep learning method," in *2019 IEEE 9th Annual International Conference on CYBER Technology in Automation, Control, and Intelligent Systems (CYBER)*, pp. 1630–1634, 2019.

[12] J. Bian, X. Hui, X. Zhao, and M. Tan, "A Novel monocular-based navigation approach for UAV autonomous transmission-line inspection," in *2018 IEEE/RSJ International Conference on Intelligent Robots and Systems (IROS)*, pp. 1–7, 2018.

[13] A. Savva, A. Zacharia, R. Makrigiorgis, A. Anastasiou, C. Kyrkou, P. Kolios, C. Panayiotou, and T. Theocharides, "ICARUS: Automatic Autonomous Power Infrastructure Inspection with UAVs," in *2021 International Conference on Unmanned Aircraft Systems (ICUAS)*, pp. 918–926, 2021.

[14] R. McLaughlin, "Extracting transmission lines from airborne LIDAR data," *IEEE Geoscience and Remote Sensing Letters*, vol. 3, no. 2, pp. 222–226, 2006.

[15] G. Sohn, Y. Jwa, and H. B. Kim, "Automatic powerline scene classification and reconstruction using airborne lidar data," *ISPRS Annals of the Photogrammetry, Remote Sensing and Spatial Information Sciences*, vol. I-3, pp. 167–172, 2012.

[16] C. Ko, T. K. Remmel, and G. Sohn, "Mapping tree genera using discrete LiDAR and geometric tree metrics," *Bosque (Valdivia)*, vol. 33, pp. 313–319, 00 2012.

[17] B. Guo, X. Huang, F. Zhang, and G. Sohn, "Classification of airborne laser scanning data using JointBoost," *ISPRS Journal of Photogrammetry and Remote Sensing*, vol. 100, pp. 71–83, 2015. High-Resolution Earth Imaging for Geospatial Information.

[18] R. Blomley, B. Jutzi, and M. Weinmann, "Classification of airborne laser scanning data using geometric multi-scale features and different neighbourhood types," *ISPRS annals*, no. 3, pp. 169–176, 2016. 12.04; LK 01.

[19] Y. Wang, Q. Chen, K. Li, D. Zheng, and J. Fang, "Airborne lidar power line classification based on spatial topological structure characteristics," *ISPRS Annals of the Photogrammetry, Remote Sensing and Spatial Information Sciences*, vol. IV-2/W4, pp. 165–169, 2017.

[20] N. Munir, M. Awrangjeb, and B. Stantic, "An Automated Method for Individual Wire Extraction from Power Line Corridor using LiDAR Data," in *2019 Digital Image Computing: Techniques and Applications (DICTA)*, pp. 1–8, 2019.

[21] S. Ortega, A. Trujillo, J. M. Santana, J. P. Suárez, and J. Santana, "Characterization and modeling of power line corridor elements from LiDAR point clouds," *ISPRS Journal of Photogrammetry and Remote Sensing*, vol. 152, pp. 24–33, 2019.

[22] S. Zorzi, E. Maset, A. Fusiello, and F. Crosilla, "Full-Waveform Airborne LiDAR Data Classification Using Convolutional Neural Networks," *IEEE Transactions on Geoscience and Remote Sensing*, vol. 57, no. 10, pp. 8255–8261, 2019.

[23] S. Pu, L. Xie, M. Ji, Y. Zhao, W. Liu, L. Wang, Y. Zhao, F. Yang, and D. Qiu, "Real-time powerline corridor inspection by edge computing of UAV lidar data," *The International Archives of the Photogrammetry, Remote Sensing and Spatial Information Sciences*, vol. XLII-2/W13, pp. 547–551, 2019.

[24] N. Munir, M. Awrangjeb, and B. Stantic, "An improved method for pylon extraction and vegetation encroachment analysis in high voltage transmission lines using LiDAR data," in *2020 Digital Image Computing: Techniques and Applications (DICTA)*, pp. 1–8, 2020.

[25] C. Nardinocchi, M. Balsi, and S. Esposito, "Fully automatic point cloud analysis for powerline corridor mapping," *IEEE Transactions on Geoscience and Remote Sensing*, vol. 58, no. 12, pp. 8637–8648, 2020.

[26] J. Redmon, S. Divvala, R. Girshick, and A. Farhadi, "You only look once: Unified, real-time object detection," in *2016 IEEE Conference on Computer Vision and Pattern Recognition (CVPR)*, pp. 779–788, 2016.

[27] T. J. Pingel, K. C. Clarke, and W. A. McBride, "An improved simple morphological filter for the terrain classification of airborne LIDAR data," *ISPRS Journal of Photogrammetry and Remote Sensing*, vol. 77, pp. 21–30, 2013.

[28] R. B. Rusu, Z. C. Marton, N. Blodow, M. Dolha, and M. Beetz, "Towards 3D Point cloud based object maps for household environments," *Robotics and Autonomous Systems*, vol. 56, no. 11, pp. 927–941, 2008. Semantic Knowledge in Robotics.

[29] M. Weinmann, B. Jutzi, S. Hinz, and C. Mallet, "Semantic point cloud interpretation based on optimal neighborhoods, relevant features and efficient classifiers," *ISPRS Journal of Photogrammetry and Remote Sensing*, vol. 105, pp. 286–304, 2015.

[30] R. B. Rusu, *Semantic 3D Object Maps for Everyday Robot Manipulation*, ch. 6: Clustering and Segmentation, pp. 78–79. Springer Tracts in Advanced Robotics, Springer Berlin, Heidelberg, 1st ed., 2013.

[31] PDAL, "PDAL - Height Above Ground Delaunay filter." Available at https://pdal.io/en/2.5.2/stages/filters.hag_delaunay.html, 11 Apr 2023.

[32] S. Guinard and L. Landrieu, "Weakly supervised segmentation-aided classification of urban scenes from 3d lidar point clouds," *The International Archives of the Photogrammetry, Remote Sensing and Spatial Information Sciences*, vol. XLII-1/W1, pp. 151–157, 2017.

[33] J. Demantké, C. Mallet, N. David, and B. Vallet, "Dimensionality based scale selection in 3D LIDAR point clouds," *ISPRS - International Archives of the Photogrammetry, Remote Sensing and Spatial Information Sciences*, vol. 3812, pp. 97–102, 2012.

[34] R. B. Rusu, *Semantic 3D Object Maps for Everyday Robot Manipulation*, ch. 4: 3D Point Feature Representations, pp. 40–41. Springer Tracts in Advanced Robotics, Springer Berlin, Heidelberg, 1st ed., 2013.